J. Phys.: Condens. Matter **21** (2009) 115902 (7pp) doi:10.1088/0953-8984/21/11/115902

High tunability of the soft mode in strained $SrTiO_3/DyScO_3$ multilayers

C Kadlec[1], F Kadlec[1], H Němec[1], P Kužel[1,4], J Schubert[2,3] and G Panaitov[2,3]

[1] Institute of Physics, Academy of Sciences of the Czech Republic, Na Slovance 2, 182 21 Prague 8, Czech Republic
[2] Institute of Bio and Nanosystems, Research Center Jülich, D-52425 Jülich, Germany
[3] Jülich Aachen Research Alliance-Fundamentals of Future Information Technology, Germany

E-mail: kuzelp@fzu.cz

Received 19 December 2008, in final form 29 January 2009
Published 20 February 2009
Online at stacks.iop.org/JPhysCM/21/115902

Abstract

$SrTiO_3/DyScO_3$ epitaxial multilayers with variable number and thickness (10–100 nm) of bilayers deposited on $DyScO_3$ substrates were investigated by means of time-domain terahertz spectroscopy at room temperature. A tensile strain develops in the $SrTiO_3$ films and shifts the eigenfrequency of the ferroelectric soft mode down by ~25–45 cm^{-1} with respect to the value found for single crystals. In all films the soft mode strongly hardens upon the electrical bias and a linear coupling to a silent excitation of relaxation type at 10 cm^{-1} is observed. We show that the change in the THz and sub-THz response of the layers with an increasing field is determined solely by the soft mode eigenfrequency and we propose a phenomenological model describing the origin of the tunability and the peculiar properties of the ferroelectric soft mode in the terahertz spectral range.

(Some figures in this article are in colour only in the electronic version)

1. Introduction

Displacive ferroelectrics are characterized by the existence of a strong polar soft lattice vibrational mode responsible for the ferroelectric phase transition [1]. Single crystals of strontium titanate (STO) exhibit typical behavior of a displacive incipient ferroelectric material, which means that, on the one hand, the dielectric behavior of STO is fully controlled by the soft mode dynamics, and on the other hand, the compound remains paraelectric down to 0 K due to quantum fluctuations [2]. These properties along with the possibility of preparing high quality thin films make STO a material of choice for applications in tunable microwave and terahertz components [3–6].

An increased room temperature tunability of STO-based structures in the microwave or THz range can be achieved either by chemical substitution of strontium atoms by barium (barium strontium titanate solid solutions) [3] or by introducing a tensile strain related to a particular choice of substrate for the epitaxial thin film growth [7]. In particular, thin STO films grown on (110) $DyScO_3$ (DSO) substrates were demonstrated to exhibit a ferroelectric phase transition close to the room temperature and, consequently, to show a highly enhanced dielectric tunability [7–12].

The contribution of the soft mode to the low frequency dielectric permittivity is dominant owing to its strongly polar character and very low frequency ω_0:

$$\Delta\varepsilon = \frac{f}{\omega_0^2}, \tag{1}$$

where f is the oscillator strength proportional to the square of the effective charge associated with the soft mode eigenvector. The tuning of the dielectric function by an applied bias E in the sub-THz range is then enabled by the strongly anharmonic character of the soft mode [13, 14] leading to $\omega_0(E)$ dependence. The bare soft mode frequency $\omega_0(E = 0)$ is determined by the in-plane strain which strongly couples to the polarization and by the sample temperature. The actual values of these two parameters define the working point for the field-induced tuning of the low frequency dielectric properties of STO which may then find applications e.g. in tunable photonic crystals [15] or metamaterials.

[4] Author to whom any correspondence should be addressed.

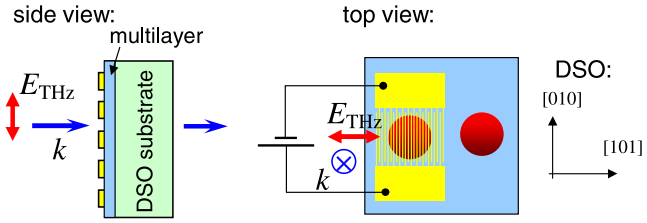

Figure 1. Scheme of the sample geometry and of the incident THz electric field and wavevector. In the top view two positions of the beam waist are shown corresponding to the measurements of the equilibrium dielectric function (position outside the electrode pattern) and of the field-induced changes (position inside the electrode pattern).

Recently a new mode of relaxation type (central mode) has been observed in strained STO films deposited on DSO substrates [6]. The origin of the coexistence of such a central mode and the soft mode close to phase transitions considered as displacive in many perovskite ferroelectrics is still a subject of scientific discussion. Recently an *ab initio* modeling supported by THz experimental data has demonstrated its close relation to the anharmonicity of the soft mode potential in the ferroelectric $BaTiO_3$ [16, 17].

In this paper we present experimental data of terahertz electric field tunability of strained multilayer structures with several thicknesses of STO layers (10, 50 and 100 nm) which may exhibit a different degree of structural relaxation and, consequently, a different strain. We show that all these structures exhibit common spectral features and we develop a general model of their behavior based on the assumed leading role of the soft mode.

2. Experimental details

The STO/DSO thin film multilayers were prepared by pulsed laser deposition (PLD) on (110)-oriented $10 \times 10 \times 0.9$ mm^3 DSO substrates. PLD growth took place in an on-axis geometry using a KrF excimer laser with a wavelength of 248 nm, a pulse width of 25 ns and a fluence of 2.5 J cm^{-2} [18]. An STO single crystal and a DSO polycrystal were used as targets. The DSO substrates were positioned directly onto a SiC resistive heater, and a molecular oxygen partial pressure of 2×10^{-1} Pa was maintained during the deposition.

An interdigitated structure of gold electrode capacitors with an area of 6×6 mm^2 and consisting of 5 μm wide metallic fingers separated by 15 μm wide gaps was deposited on top of the thin film multilayers so that it covered about one half of the sample surface. These electrodes were prepared by standard lift-off photolithography using 20 nm thick Nb/300 nm thick Au films deposited by dc magnetron sputtering. The electrode fingers were parallel to the [010] direction of the DSO substrate in the notation of [12]. Such structure of parallel wires exhibits highly anisotropic THz properties and it is transparent for THz pulses with the electric field parallel to [101] direction which was used in our experiments. The experimental scheme described is shown in figure 1.

The experiments were performed by using THz time-domain spectroscopy [19]. Like in [6], special attention has been paid to the DSO substrate preparation in order to obtain accurate dielectric spectra of the thin films. The phase delay that the THz pulse acquires due to propagation through the substrate is much larger than that due to the propagation through the thin film. The uncertainty in the transmittance phase owing to the propagation through the substrate then should be kept as small as possible. The error in the refractive index Δn of the thin film due to the phase uncertainty reads [20]

$$\Delta n \approx n_s \frac{\Delta d_s}{d} + \frac{|d_s - d_r|}{d} \Delta n_s, \qquad (2)$$

where d is the film thickness, Δd_s is the error in the substrate thickness determination, Δn_s is the uncertainty in its refractive index, and d_s, d_r are the thicknesses of the substrate under the thin film and of the reference (bare) substrate, respectively. The second term on the right-hand side of (2) can be neglected if all the prepared substrates have the same thickness with approximately micrometer precision. The magnitude of the first term critically depends on the substrate plane parallelism and on the accuracy of its thickness determination. Note that in our experimental situation with $n_s = 4.5$ and $d = 200$ nm one would obtain $\Delta n \approx 20$ even for $\Delta d_s \approx 1$ μm; consequently, a better accuracy was required in our experiments.

We first mechanically polished a series of $10 \times 10 \times 0.85$ mm^3 DSO substrates to highly plane parallel plates with optical quality of surfaces and with the same thickness (within 2 μm precision). Subsequently we have measured their THz refractive index spectra and refined their thickness determination by using the fact that the internal Fabry–Pérot reflections in the substrate are resolved in time and form distinct THz echoes. A separate analysis of these echoes allows one to find the optimum thicknesses of the substrates with respect to the THz measurements with ~200 nm precision [21]. These thickness values were used subsequently after the thin film deposition for the determination of dielectric properties of STO. With these preparations we estimate at most a 20% error in the determination of the absolute value of the permittivity of our films.

The following samples were studied:

- a single 100 nm thick STO layer (sample 1×100C);
- multilayers consisting of n STO/DSO bilayers ($n = 2, 3, 4$) where the thickness of each layer was 50 nm, i.e. the total thickness of STO was 100, 150 and 200 nm, respectively (samples 2×50, 3×50, 4×50); the upper layer was STO for each of these samples;
- a multilayer consisting of 20 STO/DSO bilayers where the thickness of each layer was 10 nm, i.e. the total thickness of STO was 200 nm (sample 20×10); the upper layer was DSO.

The THz time-domain experiments were performed with the help of a Ti:sapphire oscillator (Coherent, Mira) as a femtosecond laser source. For the generation of linearly polarized THz probing pulses we used an interdigitated photoconducting switch [22] and for their detection we applied the usual phase-sensitive electro-optic sampling scheme with a 1 mm thick [110] ZnTe crystal and a pair of balanced photodiodes [23].

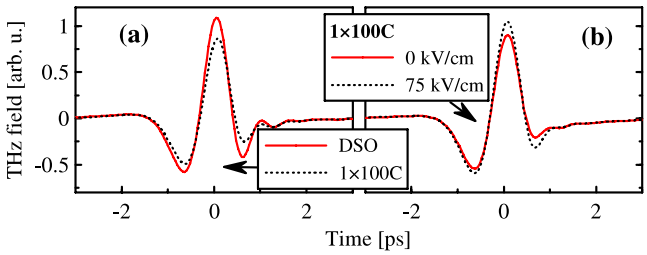

Figure 2. Examples of the measured THz wave forms. (a) Equilibrium properties: wave form transmitted through a bare DSO substrate (reference E_r, solid line) and through DSO with the film 1 × 100C (E_s, dotted line). (b) Field-induced properties: wave form transmitted through a 1 × 100C sample without bias (reference E_0, solid) and with the bias (E_V, dotted).

3. Experimental results

First we determined the complex dielectric spectra of the STO layers without electric bias. For this purpose the THz beam was sent to the parts of the samples without electrodes (see figure 1). The experiments consisted of two consecutive measurements: one of a signal wave form $E_s(t)$ using a sample with the thin film structure and one of a reference wave form $E_r(t)$ with a bare DSO substrate (figure 2(a)). The ratio of the Fourier transforms of the time-domain waveforms provides the complex THz transmittance spectrum of the film: $t(\omega) = E_s(\omega)/E_r(\omega)$. An example of the complex transmission function is shown in figure 3.

The optical thicknesses of all the films within the investigated multilayers were much smaller than the wavelength of the THz radiation. The effective medium approach is then fully justified for the evaluation of the dielectric function of STO thin films from the experimental data. From this point of view the THz transmission through an STO/DSO multilayer is equivalent to the transmission through an STO/DSO bilayer with the summed thicknesses of each material. We verified the validity of this approach using the transfer matrix formalism for layered media [24] by calculating and comparing the transmission functions for the THz propagation through a multilayer and through the equivalent bilayer. We also verified experimentally that the field-induced changes of the dielectric function of DSO are quite negligible. The evaluation of the THz dielectric properties from the measured transmission function can then be performed by assuming a sample geometry with a single STO layer on top of a DSO substrate (both with appropriate thicknesses). The complex refractive index $N = n + i\kappa$ of the STO films is then determined by numerically inverting the expression

$$t(\omega) = \frac{2N(N_s+1)\exp[ik_0(N-1)d]\exp[ik_0(N_s-1)(d_s-d_r)]}{(1+N)(N+N_s)+(1-N)(N-N_s)\exp[2ik_0Nd]}, \quad (3)$$

where d is the total thickness of STO in the multilayer, $N_s = n_s + i\kappa_s$ is the complex refractive index of DSO, and $k_0 = \omega/c$ with c denoting the speed of light in vacuum. The complex dielectric response of STO $\varepsilon = N^2$ is then evaluated under the assumption of a uniformly strained STO. The possible gradient of dielectric properties related to the strain gradient along the multilayer would result in an inhomogeneous broadening of the retrieved spectral features.

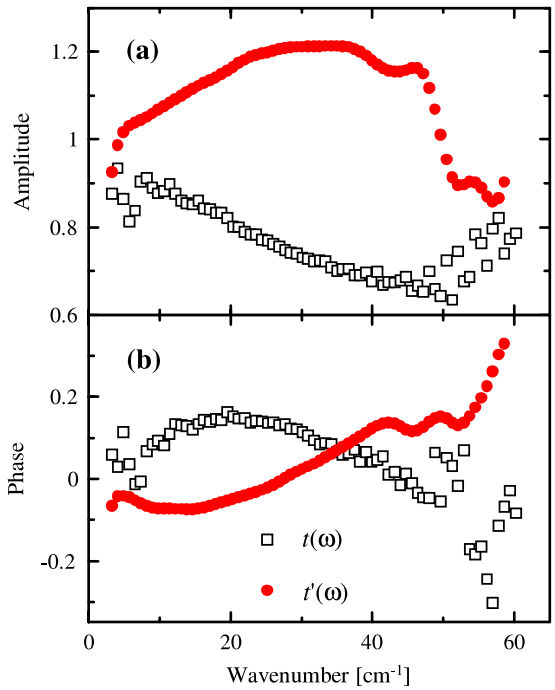

Figure 3. Amplitude (a) and phase (b) of equilibrium (squares) and field-induced (circles) transmission functions t and t', respectively, for the sample 1 × 100C. Field value: 75 kV cm^{-1}. In the case of t (equilibrium, $E = 0$) the reference is the bare substrate; in the case of t' the reference is the measurement with $E = 0$.

The measured zero-field dielectric functions of all the samples investigated are shown in figure 4. Note that the spectra for samples where the individual STO layers are thicker (samples 1 × 100C and n × 50) are quite similar to each other, reaching a permittivity of about 1500 near 10 cm^{-1} and showing rather broad features in the losses. In contrast, the real part of the permittivity of the 20 × 10 sample shows a different slope and does not exceed 1000; the losses are then significantly lower.

In the second series of experiments we investigated field-induced changes of the dielectric function. In these experiments various values of a dc bias E were applied to the samples and the THz transmission spectra were measured. Here the reference THz wave forms $E_0(t)$ were measured with the electric field off and the signal wave forms $E_V(t)$ were obtained with the applied bias: $t'(\omega) = E_V(\omega)/E_0(\omega)$ (see examples in figures 2(b) and 3). Note that the amplitude of t' exceeds unity in a broad spectral range which means that the thin film becomes more transparent upon applying the bias. The calculation of the refractive index N' and of the related dielectric function under the external bias was accomplished by inverting the following expression for the transmission function:

$$t'(\omega) = \frac{N'}{N}\{(1+N)(N+N_s)\exp[-ik_0Nd] + (1-N)(N-N_s)\exp[ik_0Nd]\}$$

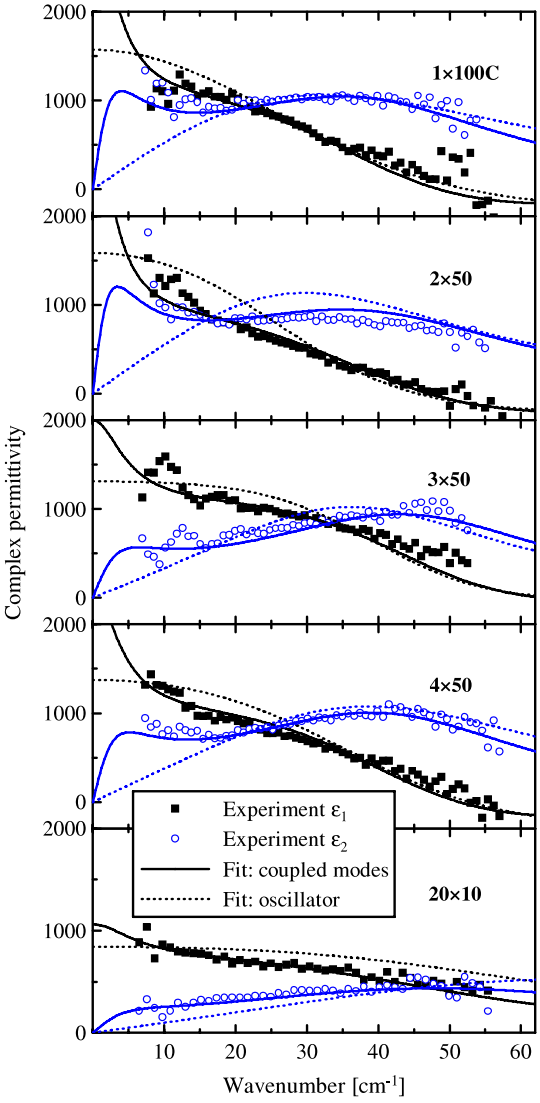

Figure 4. Zero-field dielectric spectra ($\varepsilon = \varepsilon_1 + \mathrm{i}\varepsilon_2$) of the STO layers. Symbols: experiment; solid lines: fits with the coupled mode formula (7); dotted lines: fits with an oscillator model.

$$\times \left\{(1+N')(N'+N_\mathrm{s})\exp[-\mathrm{i}k_0N'd] + (1-N')(N'-N_\mathrm{s})\exp[\mathrm{i}k_0N'd]\right\}^{-1}. \quad (4)$$

In our measurements we applied bias voltages in the range 0–112 V which correspond to the in-plane fields of 0–75 kV cm^{-1}. Examples of the measured dielectric spectra of biased samples are shown in figure 5.

4. Discussion

In order to describe the measured spectra we consider (similarly to [6, 17]) a pair of linearly coupled lattice modes (with a coupling constant δ): a damped oscillator (standing for the soft mode with a bare eigenfrequency ω_0, damping Γ and strength f) and a Debye relaxation (central mode with a relaxation frequency γ). The formula describing the permittivity can be written as follows:

$$\varepsilon(\omega) = S_iS_j\boldsymbol{G}_{ij}(\omega) + \varepsilon_\infty \quad (5)$$

where ε_∞ is the high frequency permittivity, $\boldsymbol{G}(\omega)$ is a Green function matrix of the coupled modes:

$$\boldsymbol{G}^{-1}(\omega) = \begin{pmatrix} 1-\mathrm{i}\omega/\gamma & \delta \\ \delta & \omega_0^2-\omega^2-\mathrm{i}\omega\Gamma \end{pmatrix}, \quad (6)$$

and the components S_i are proportional to the effective charge associated with the corresponding mode, or in other words, they describe the dielectric strengths of the two modes. We assume $S_1 = 0$ and $S_2 = f^{1/2}$ (cf equation (1)), which means that the relaxation is considered as a silent excitation which may be observed in the spectra only owing to its coupling to the strongly polar soft mode. One finds

$$\varepsilon(\omega) = \frac{f}{\omega_0^2-\omega^2-\mathrm{i}\omega\Gamma-\delta^2/(1-\mathrm{i}\omega/\gamma)} + \varepsilon_\infty. \quad (7)$$

This form in particular (i) emphasizes the leading role of the soft mode in the THz and sub-THz dynamics as the value of its eigenfrequency controls the apparent polar response of the relaxator in the spectra, and (ii) allows satisfying the sum rule [25] (i.e. vanishing high frequency conductivity). This demonstrates the tight relation between the two modes and one can understand the relaxation as an additional low frequency decay channel of the soft mode, i.e. as a specific anharmonicity (side minima) in the soft mode potential similarly to what was shown by *ab initio* calculations in the case of $BaTiO_3$ [16, 17]. Note, however, that no similar *ab initio* calculation which could confirm this hypothesis has been published yet for STO.

Figure 5 shows dielectric spectra of the samples studied and the fits with equation (7). Note that this formula contains six independent parameters. The value of f ($\approx 2.34 \times 10^6$ cm^{-2}) is known to be temperature independent and similar for single crystals and thin films [14]; consequently it was kept constant in our fits. Our aim was to demonstrate the universal behavior of the coupled modes in STO; therefore we assumed that the parameters γ and δ are field and sample independent (i.e. strain independent, too); in other words, all the spectra for all the samples were fitted with single values of γ (≈ 10 cm^{-1}) and δ (≈ 34 cm^{-1}). The effective soft mode damping may depend on the inhomogeneous broadening of the spectra due to the strain gradient. Therefore we allowed for each sample its own value of Γ which was then considered as field independent. The high frequency permittivity ε_∞ has the weakest physical meaning in our fits as it mainly reflects the large uncertainty in the experimental permittivity which was discussed above. Therefore this parameter was considered as field independent but again a different value was allowed for each sample.

The most important parameter obtained from the fits is the soft mode eigenfrequency which was assumed to reflect both the bias and the strain in the samples (i.e. we optimized the value of ω_0 for each spectrum); a summary of these results is displayed in figure 6. The important fit values are summarized in table 1.

In order to show unambiguously the important role of the soft mode–central mode coupling we performed fits of the data with a simple oscillator model (obtained from (7) by

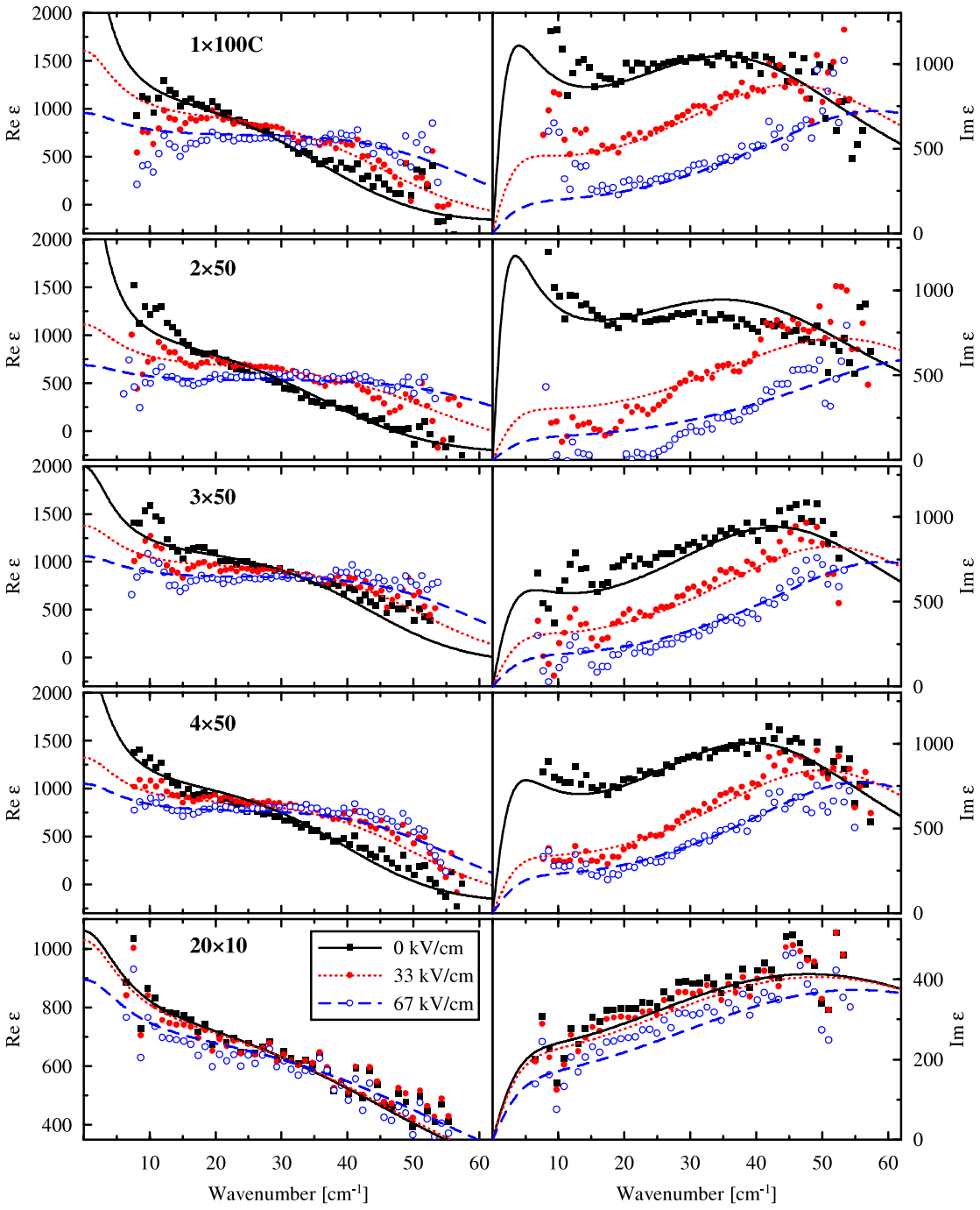

Figure 5. Dielectric spectra of all the samples investigated at room temperature for several values of the bias field. Symbols: experimental data; lines: fits using (7).

setting $\delta = 0$) and with the factorized form of the dielectric function [26] for a single oscillator:

$$\varepsilon(\omega) = \varepsilon_\infty \frac{\omega_0^2 + f/\varepsilon_\infty - \omega^2 - \mathrm{i}\omega\Gamma_\mathrm{L}}{\omega_0^2 - \omega^2 - \mathrm{i}\omega\Gamma}, \qquad (8)$$

where Γ_L is the damping of the longitudinal phonon mode. This model was also previously applied to STO single crystals in order to describe the higher frequency phonon spectra [27]. However, these fits are markedly less satisfactory at the low frequency part of the measured spectra. We performed global fits for each sample, i.e. taking into account simultaneously all the measured spectra with varying electric field, like what was described above for the coupled modes model (in addition, the oscillator strength f was also allowed to vary in these fits). Both oscillator models provide comparable fits with a variance of residuals about 30–40% higher than for the coupled modes fit. A comparison of the fits for all samples without electric bias is shown in figure 4.

As the probing THz electric field is parallel to the applied bias we can consider the simplest form of the Helmholtz free

Table 1. Summary of the measured characteristics of the thin film samples.

Sample	1 × 100C	2 × 50	3 × 50	4 × 50	20 × 10	Single crystal[a]
STO thickness [nm]	100	100	150	200	200	—
ω_0 (0 kV cm^{-1}) [cm^{-1}]	44	46	51	47	65	90
ω_0 (66 kV cm^{-1}) [cm^{-1}]	63	67	64	61	70	
Γ [cm^{-1}]	48	55	43	48	92	25
ε_0 (0 kV cm^{-1})	3050	3100	2000	2350	1050	310
ε_0 (66 kV cm^{-1})	950	700	1050	1050	900	
β [10^9 J C^{-4} m^5]	9 ± 2	22 ± 4	14 ± 2	14 ± 2	9 ± 2	8–10
γ [cm^{-1}]			10			
δ [cm^{-1}]			34			

[a] The data for STO single crystals were taken from [14]. ε_0 is the static value of the permittivity provided by the fit (not measured directly).

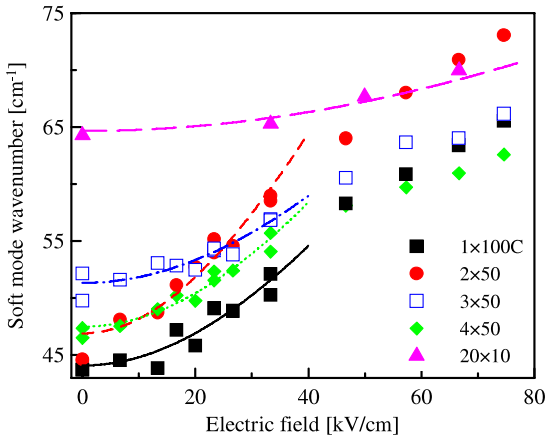

Figure 6. Electric field dependence of the soft mode eigenfrequency for the samples investigated. Symbols: ω_0 obtained from the fits of THz spectra with (7); lines: fits of the weak field data with (10).

energy expansion F to describe the soft mode behavior [3]:

$$F = \frac{\omega_0^2(0)}{2f\varepsilon_{\rm vac}}P^2 + \frac{\beta}{4}P^4, \qquad (9)$$

where $\varepsilon_{\rm vac}$ is the vacuum permittivity and the coefficient β characterizes the anharmonicity of the soft mode potential minimum. Note that the relaxation mode (which could represent e.g. transitions to a side potential minimum of the soft mode [17]) is not considered in this simplified expansion. The soft mode contribution to the dielectric permittivity given by (1) can then be characterized in the weak field limit by [14]

$$\omega_0(E) \approx \omega_0(0)\sqrt{1 + 3\beta\,[\varepsilon_{\rm vac}f/\omega_0^2(0),]^3E^2}, \qquad (10)$$

where E is the value of the electric bias. The field dependence of the soft mode frequency for all the samples investigated is shown in figure 6 along with the fits with the theoretical expression (10). In the weak field limit ($E < 35$ kV cm^{-1}) the experimental data show a good agreement with the predicted approximately quadratic behavior, which allows us to determine the anharmonic coefficient β characterizing the tuning capability of the STO layers. These values are summarized in table 1. We find that the samples 1 × 100C and 20 × 10 exhibit the same values as STO single crystals. On the other hand, the anharmonicity for $n \times 50$ samples seems to be somewhat enhanced. The highest value is found for the 2 × 50 sample (enhanced approximately by a factor of 2 compared to the single-crystal one). An intermediate value is found for the 3 × 50 sample and the value of β does not seem to decrease when a fourth STO film is added (4 × 50).

The highest total thickness of STO (200 nm) was achieved for the samples 4 × 50 and 20 × 10. However, the latter shows a significantly higher inhomogeneous broadening as demonstrated by the high value of its effective soft mode damping constant Γ and an intermediate value of its bare eigenfrequency. This suggests that the high strain in the layers next to the substrate is not maintained along the multilayer and a large strain gradient develops. This is then reflected in a relatively poor tunability of this structure. In this sense the samples with intermediate STO thickness of 50 nm seem to be the most suitable for tunable applications in the THz range. An open technological question remains, as regards whether it is possible to grow $n \times 50$ samples with $n > 4$ and still achieve an enhanced tunability with these structures.

5. Conclusion

We have characterized THz dielectric properties of several types of $SrTiO_3/DyScO_3$ multilayers at room temperature with and without electrical bias. A universal behavior of the THz spectra was observed, which was quantitatively explained by the linear coupling of the ferroelectric soft mode to a silent relaxation mode and by the anharmonicity of the soft mode potential. This anharmonicity was determined for all the structures from the experimentally observed soft mode hardening upon the applied bias.

Acknowledgments

This work was supported by the Academy of Sciences of the Czech Republic (project AVOZ10100520), by its Grant Agency (project A100100907) and by the Ministry of Education of the Czech Republic (project LC-512).

References

[1] Lines M E and Glass A M 1979 *Principles and Applications of Ferroelectrics and Related Materials* (Oxford: Clarendon)
[2] Müller K A and Burkard H 1979 *Phys. Rev.* B **19** 3593
[3] Tagantsev A K, Sherman V O, Astafiev K F, Venkatesh J and Setter N 2003 *J. Electroceram.* **11** 5
[4] Kužel P, Kadlec F, Němec H, Ott R, Hollmann E and Klein N 2006 *Appl. Phys. Lett.* **88** 102901
[5] Kužel P, Kadlec F, Petzelt J, Schubert J and Panaitov G 2007 *Appl. Phys. Lett.* **91** 232911
[6] Kužel P, Kadlec C, Kadlec F, Schubert J and Panaitov G 2008 *Appl. Phys. Lett.* **93** 052910
[7] Haeni J H, Irvin P, Chang W, Uecker R, Reiche P, Li Y L, Choudhury S, Tian W, Hawley M E, Craigo B, Tagantsev A K, Pan X Q, Streiffer S K, Chen L Q, Kirchoefer S W, Levy J and Schlom D G 2004 *Nature* **430** 758
[8] Irvin P, Levy J, Haeni J H and Schlom D G 2006 *Appl. Phys. Lett.* **88** 042902
[9] Chang W, Bellotti J A, Kirchoefer S W and Pond J M 2006 *J. Electroceram.* **17** 487
[10] Vasudevarao A, Kumar A, Tian L, Haeni J H, Li Y L, Eklund C-J, Jia Q X, Uecker R, Reiche P, Rabe K M, Chen L Q, Schlom D G and Gopalan V 2006 *Phys. Rev. Lett.* **97** 257602
[11] Heeg T, Schubert J, Buchal Ch, Cicerrella E, Freeouf J L, Tian W, Jia Y and Schlom D G 2006 *Appl. Phys.* A **83** 103
[12] Wördenweber R, Hollmann E, Kutzner R and Schubert J 2007 *J. Appl. Phys.* **102** 044119
[13] Fleury P A and Worlock J M 1968 *Phys. Rev.* **174** 613
[14] Kužel P and Kadlec F 2008 *C. R. Physique* **9** 197–214
[15] Němec H, Kužel P, Duvillaret L, Pashkin A, Dressel M and Sebastian M 2005 *Opt. Lett.* **30** 549–51
[16] Ponomareva I, Bellaiche L, Ostapchuk T, Hlinka J and Petzelt J 2008 *Phys. Rev.* B **77** 012102
[17] Hlinka J, Ostapchuk T, Nuzhnyy D, Petzelt J, Kužel P, Kadlec C, Vaněk P, Ponomareva I and Bellaiche L 2008 *Phys. Rev. Lett.* **101** 167402
[18] Beckers L, Schubert J, Zander W, Ziesmann J, Eckau A, Leinenbach P and Buchal C 1998 *J. Appl. Phys.* **83** 3305
[19] Dexheimer S L 2008 *THz Spectroscopy: Principles and Applications* (Boca Raton, FL: CRC Press)
[20] Petzelt J, Kužel P, Rychetský I, Pashkin A and Ostapchuk T 2003 *Ferroelectrics* **288** 169–85
[21] Duvillaret L, Garet F and Coutaz J-L 1996 *IEEE J. Sel. Top. Quantum Electron.* **2** 739
[22] Dreyhaupt A, Winnerl S, Dekorsy T and Helm M 2005 *Appl. Phys. Lett.* **86** 121114
[23] Nahata A, Weling A S and Heinz T F 1996 *Appl. Phys. Lett.* **69** 2321–3
[24] Pedrotti F L and Pedrotti L S 1993 *Introduction to Optics* 2nd edn (Englewood Cliffs, NJ: Prentice-Hall)
[25] Hlinka J, Petzelt J, Kamba S, Noujni D and Ostapchuk T 2006 *Phase Transit.* **79** 41
[26] Berreman D W and Unterwald F C 1968 *Phys. Rev.* **174** 791
[27] Servoin J L, Luspin Y and Gervais F 1980 *Phys. Rev.* B **22** 5501